

PL-TR-91-2179

2

AD-A241 318



MEASUREMENTS OF OCEAN SURFACE WIND SPEED
WITH THE SPECIAL SENSOR MICROWAVE/IMAGER (SSM/I)

M. A. GOODBERLET
C. T. SWIFT

DTIC
ELECTE
OCT 03 1991
S D D

University of Massachusetts
Amherst, MA 01003

26 June 1991

Final Report
April 1990 - July 1991

APPROVED FOR PUBLIC RELEASE; DISTRIBUTION UNLIMITED

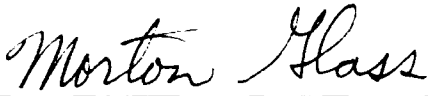


PHILLIPS LABORATORY
AIR FORCE SYSTEMS COMMAND
HANSCOM AIR FORCE BASE, MASSACHUSETTS 01731-5000

91-12641



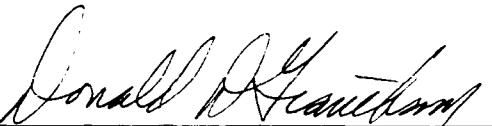
This technical report has been reviewed and is approved for publication.



MORTON GLASS
Contract Manager



JOSEPH W. SNOW, Chief
Satellite Meteorology Branch
Atmospheric Sciences Division



DONALD D. GRANTHAM
Acting Director
Atmospheric Sciences Division

This document has been reviewed by the ESD Public Affairs Office (PA) and is releasable to the National Technical Information Service (NTIS).

Qualified requestors may obtain additional copies from the Defense Technical Information Center. All others should apply to the National Technical Information Service.

If your address has changed, or if you wish to be removed from the mailing list, or if the addressee is no longer employed by your organization, please notify PL/IMA, Hanscom AFB, MA 01731-5000. This will assist us in maintaining a current mailing list.

Do not return copies of this report unless contractual obligations or notices on a specific document requires that it be returned.

REPORT DOCUMENTATION PAGE			Form Approved OMB No 0704-0188	
<small>Public reporting burden for this collection of information is estimated to average 1 hour per response, including the time for reviewing instructions, searching existing data sources, gathering and maintaining the data needed, and completing and reviewing the collection of information. Send comments regarding this burden estimate or any other aspect of this collection of information, including suggestions for reducing this burden, to Washington Headquarters Services, Directorate for Information Operations and Reports, 1215 Jefferson Davis Highway, Suite 1204, Arlington, VA 22202-4302, and to the Office of Management and Budget, Paperwork Reduction Project (0704-0188), Washington, DC 20503.</small>				
1. AGENCY USE ONLY (Leave blank)	2. REPORT DATE 26 June 1991	3. REPORT TYPE AND DATES COVERED Final (April 1990 - July 1991)		
4. TITLE AND SUBTITLE Measurements of Ocean Surface Wind Speed With The Special Sensor Microwave/Imager (SSM/I)		5. FUNDING NUMBERS PE 63707F PR 2688 TA 04 WU KG Contract F19628-90-K-0034		
6. AUTHOR(S) M. A. Goodberlet C. T. Swift				
7. PERFORMING ORGANIZATION NAME(S) AND ADDRESS(ES) University of Massachusetts Amherst, MA 01003		8. PERFORMING ORGANIZATION REPORT NUMBER		
9. SPONSORING / MONITORING AGENCY NAME(S) AND ADDRESS(ES) Phillips Laboratory Hanscom AFB, MA 01731-5000 Contract Manager: Morton Glass/LYS		10. SPONSORING / MONITORING AGENCY REPORT NUMBER PL-TR-91-2179		
11. SUPPLEMENTARY NOTES				
12a. DISTRIBUTION / AVAILABILITY STATEMENT Approved for public release; distribution unlimited			12b. DISTRIBUTION CODE	
13. ABSTRACT (Maximum 200 words) An improved algorithm which can be used to estimate ocean surface wind speed from radiometric data collected by the Defense Meteorological Space Program's (DMSP) Special Sensor Microwave/Imager (SSM/I) is proposed. As compared to the previous DMSP wind speed algorithm, retrievals of the improved algorithm are unbiased under a wider range of weather conditions. The improved algorithm also calculates accuracy flags which indicate the specific accuracy of each wind speed retrieval. A retrieval accuracy of better than 2 m/s for over 85% of the global wind speed measurements can be expected.				
14. SUBJECT TERMS Remote sensing, Microwave, Ocean-Atmosphere Interactions, Satellites			15. NUMBER OF PAGES 38	
			16. PRICE CODE	
17. SECURITY CLASSIFICATION OF REPORT Unclassified	18. SECURITY CLASSIFICATION OF THIS PAGE Unclassified	19. SECURITY CLASSIFICATION OF ABSTRACT Unclassified	20. LIMITATION OF ABSTRACT SAR	

TABLE OF CONTENTS

LIST OF FIGURES	iv
LIST OF TABLES	vii
Section	
1. Purpose	1
2. Background	1
3. Problem Description and Goals of the Study	1
4. Methodology	7
5. Merged Data Set and Comparison Criteria	9
6. SFMR Calibration	12
7. Results	12
8. Discussion and Conclusions	28
Acknowledgements	28
References	29

Accession For	
NTIS CRA&I	<input checked="" type="checkbox"/>
DTIC TAB	<input type="checkbox"/>
Unannounced	<input type="checkbox"/>
Justification	
By	
Distribution /	
Availability Codes	
Dist	Avail and/or Special
A-1	

LIST OF FIGURES

Fig. 3.1	Standard deviation (ie. random error), SD, and bias of the SSM/I wind speed retrievals from the ERT D-matrix algorithm plotted as a function of the "true" wind speed measured by NOAA ocean buoys.	3
Fig. 3.2	Standard deviation (ie. random error), SD and bias of the SSM/I wind speed retrievals from the Global D-matrix algorithm plotted as a function of the "true" wind speed measured by NOAA ocean buoys. The SSM/I brightness temperature difference, $T_B(37V) - T_B(37H)$, for data used to create this plot was always greater than 52 K.	4
Fig. 3.3	Standard deviation (ie. random error), SD, and bias of the SSM/I wind speed retrievals from the Global D-matrix algorithm plotted as a function of the the SSM/I brightness temperature difference, $T_B(37V) - T_B(37H)$	5
Fig. 4.1	The difference between SSM/I and NOAA buoy measured wind speed plotted against the SSM/I brightness temperature difference, $T_B(37V) - T_B(37H)$, for the 3982 data pairs of the SSM/I-buoy merged data file.	8
Fig. 5.1	Histogram of SSM/I brightness temperature difference, $T_B(37V) - T_B(37H)$, for the 3982 data pairs of the SSM/I-NOAA buoy merged data file.	10
Fig. 5.2	Histogram of the NOAA buoy measured wind speed for the 3982 data pairs of the SSM/I-buoy merged data file.	11
Fig. 5.3	Histogram of SSM/I brightness temperature difference, $T_B(37V) - T_B(37H)$, for the 200 data pairs of the SSM/I-SFMR merged data file.	14
Fig. 5.4	Histogram of the SFMR measured wind speed for the 200 data pairs of the SSM/I-SFMR merged data file.	15
Fig. 7.1	The difference between SSM/I and NOAA buoy measured wind speed plotted against the SSM/I brightness temperature difference, $T_B(37V) - T_B(37H)$, for the 1442 data pairs of the SSM/I-buoy merged data file where the buoy measured wind speed is between 0 and 6 m/s.	16

- Fig. 7.2 The difference between SSM/I and NOAA buoy measured wind speed plotted against the SSM/I brightness temperature difference, $T_B(37V) - T_B(37H)$, for the 2044 data pairs of the SSM/I-buoy merged data file where the buoy measured wind speed is between 6 and 12 m/s 17
- Fig. 7.3 The difference between SSM/I and NOAA buoy measured wind speed plotted against the SSM/I brightness temperature difference, $T_B(37V) - T_B(37H)$, for the 496 data pairs of the SSM/I-buoy merged data file where the buoy measured wind speed is greater than 12 m/s 18
- Fig. 7.4 The difference between SSM/I and SFMR measured wind speed plotted against the SSM/I brightness temperature difference, $T_B(37V) - T_B(37H)$, for the 140 data pairs of the SSM/I-SFMR merged data file where the SFMR measured wind speed is greater than 15 m/s . The "+" marks indicate data from tropical regions and the "o" marks indicates data from a storm near the Gulf of Alaska (see Table 2) 19
- Fig. 7.5 Standard deviation (ie. random error), SD, and bias of SSM/I wind speed retrievals from the GSW algorithm made under high ($> 12 m/s$) wind speed conditions plotted as a function of the SSM/I brightness temperature difference, $T_B(37V) - T_B(37H)$. Data used to construct this plot consisted of only SSM/I-buoy coincident data pairs. . . . 22
- Fig. 7.6 Standard deviation (ie. random error), SD, and bias of SSM/I wind speed retrievals from the GSW algorithm made under medium (6–12 m/s) wind speed conditions plotted as a function of the SSM/I brightness temperature difference, $T_B(37V) - T_B(37H)$. Data used to construct this plot consisted of only SSM/I-buoy coincident data pairs. . . . 23
- Fig. 7.7 Standard deviation (ie. random error), SD, and bias of SSM/I wind speed retrievals from the GSW algorithm made under low (0–6 m/s) wind speed conditions plotted as a function of the SSM/I brightness temperature difference, $T_B(37V) - T_B(37H)$. Data used to construct this plot consisted of only SSM/I-buoy coincident data pairs. . . . 24

- Fig. 7.8 Scatter-plot of SSM/I wind speed estimates from the GSW algorithm and coincident wind speed measurements from NOAA buoys 46035 and 46001 made during the time period 1Sep87 through 1Mar88. The SSM/I brightness temperature difference, $T_B(37V) - T_B(37H)$, for data used to create this plot was always greater than 35 K. 25
- Fig. 7.9 Scatter-plot of SSM/I wind speed estimates from the GSW algorithm and coincident wind speed measurements from NOAA buoys 42001 and 42002 made during the time period 1Sep87 through 1Mar88. The SSM/I brightness temperature difference, $T_B(37V) - T_B(37H)$, for data used to create this plot was always greater than 35 K. 26
- Fig. 7.10 Scatter-plot of SSM/I wind speed estimates from the GSW algorithm and coincident wind speed measurements made by NOAA buoys and the SFMR under high ($> 12 \text{ m/s}$) wind speed conditions. Points marked with a dot represent SSM/I-buoy comparisons. Points marked with a plus sign represent SSM/I-SFMR comparisons in tropical regions and points marked with a circle represent SSM/I-SFMR comparisons in a storm near the Gulf of Alaska (see Table 2). The SSM/I brightness temperature difference, $T_B(37V) - T_B(37H)$, for data used to create this plot was always greater than 35 K. 27

LIST OF TABLES

Table 1.	Specifications of the global D-matrix wind speed algorithm where the calculated wind speed, W , is in meters per second and referenced to a height of 19.5 meters above the ocean surface.	2
Table 2.	Stepped Frequency Microwave Radiometer (SFMR) flights which were colocated with wind speed measurements of the Special Sensor Microwave/Imager (SSM/I).	13
Table 3.	Specifications of the GSW wind speed algorithm where the calculated wind speed, W , is in meters per second and referenced to a height of 19.5 meters above the ocean surface. <i>Under no conditions should this algorithm be used when the Δ_{37} differential is less than 31 K.</i>	21

1. Purpose

To describe an improved algorithm which can be used to estimate ocean surface wind speed from radiometric data collected by the Defense Meteorological Space Program's (DMSP) Special Sensor Microwave/Imager (SSM/I) Block 5D-2 Spacecraft F8.

2. Background

Environmental Research Technology Inc. (ERT) under contract from Hughes Aircraft developed the D-matrix algorithm [Lo, 1983] for the purpose of converting the over-ocean brightness temperature measurements, T_B , of the SSM/I into estimates of the "true" wind (hereafter defined as an 8.5-minute time-average of the wind field at an altitude of 19.5 meters above the ocean surface). The D-matrix algorithm was tested during the DMSP Calibration/Validation effort [Hollinger et al., 1989] and an improved algorithm was created and is described in Table 1 and by [Goodberlet et al., 1989]. Note that the improved D-matrix algorithm (hereafter referred to as the Global D-matrix algorithm) makes use of the SSM/I brightness temperature measurements at 19 GHz-vertical polarization, $T_B(19V)$, 22 GHz-vertical polarization, $T_B(22V)$, 37 GHz-vertical polarization, $T_B(37V)$, and at 37 GHz-horizontal polarization, $T_B(37H)$.

A unique feature of the D-matrix concept is that the accuracy of each wind speed retrieval is indicated by an accuracy flag (originally called "rain flag" by ERT) between 0 and 3 (see Table 1). Note that the accuracy flag is set based on the brightness temperature difference, $\Delta_{37} = T_B(37V) - T_B(37H)$, and on the level of $T_B(19H)$. As an example of using the accuracy flags, suppose that the D-matrix algorithm reports a wind speed of 15 m/s with accuracy flag 0. Using Table 1, it is found that the retrieval is accurate to within 2 m/s (ie. one can be 68% certain that the actual wind speed, in this example, is between 13 and 17 m/s). This interpretation of the accuracy flag is strictly valid only when the retrieved wind speeds are unbiased and, as discussed below, the Global D-matrix algorithm retrievals are only unbiased under accuracy flag 0 conditions.

The effects of atmospheric water (ie. water vapor, clouds or rain) upon the SSM/I measurements degrades the accuracy of the D-matrix wind speed retrievals. Therefore, the higher accuracy flags, which are associated with the smaller values of Δ_{37} , indicate higher retrieval error and the fact that the SSM/I made the measurement through a water-laden atmosphere.

3. Problem Description and Goals of the Study

A deficiency of the original ERT D-matrix algorithm was that it overestimated low winds and underestimated high winds; a condition which is summarized by the curve labelled "BIAS" in Figure 3.1. The DMSP Calibration/Validation effort resulted in the Global D-matrix algorithm whose wind speed estimates are nearly unbiased under accuracy flag 0 conditions (see Figures 3.2 and 3.3). However, as shown in Figure 3.3, retrievals of the Global D-matrix algorithm tend to be biased high under accuracy flag 1, 2 and 3 conditions (ie. when the Δ_{37} differential is less than 50 K). This bias (hereafter called the weather-bias) also depends upon wind speed itself and, as shown in section 7, can be

Table 1. Specifications of the global D-matrix wind speed algorithm where the calculated wind speed, W , is in meters per second and referenced to a height of 19.5 meters above the ocean surface.

$$W = 147.90 + 1.0969 \cdot T_B(19V) - 0.4555 \cdot T_B(22V) - 1.7600 \cdot T_B(37V) + 0.7860 \cdot T_B(37H)$$

<u>Accuracy Flag</u>	<u>Criteria</u>	<u>Accuracy (m/s)</u>
0	$\Delta_{37} > 50$ $T_B(19H) < 165$	< 2
1	$37 < \Delta_{37} < 50$ $T_B(19H) > 165$	$2 - 5$
2	$30 < \Delta_{37} < 37$	$5 - 10$
3	$\Delta_{37} < 30$	> 10

$$\Delta_{37} = T_B(37V) - T_B(37H)$$

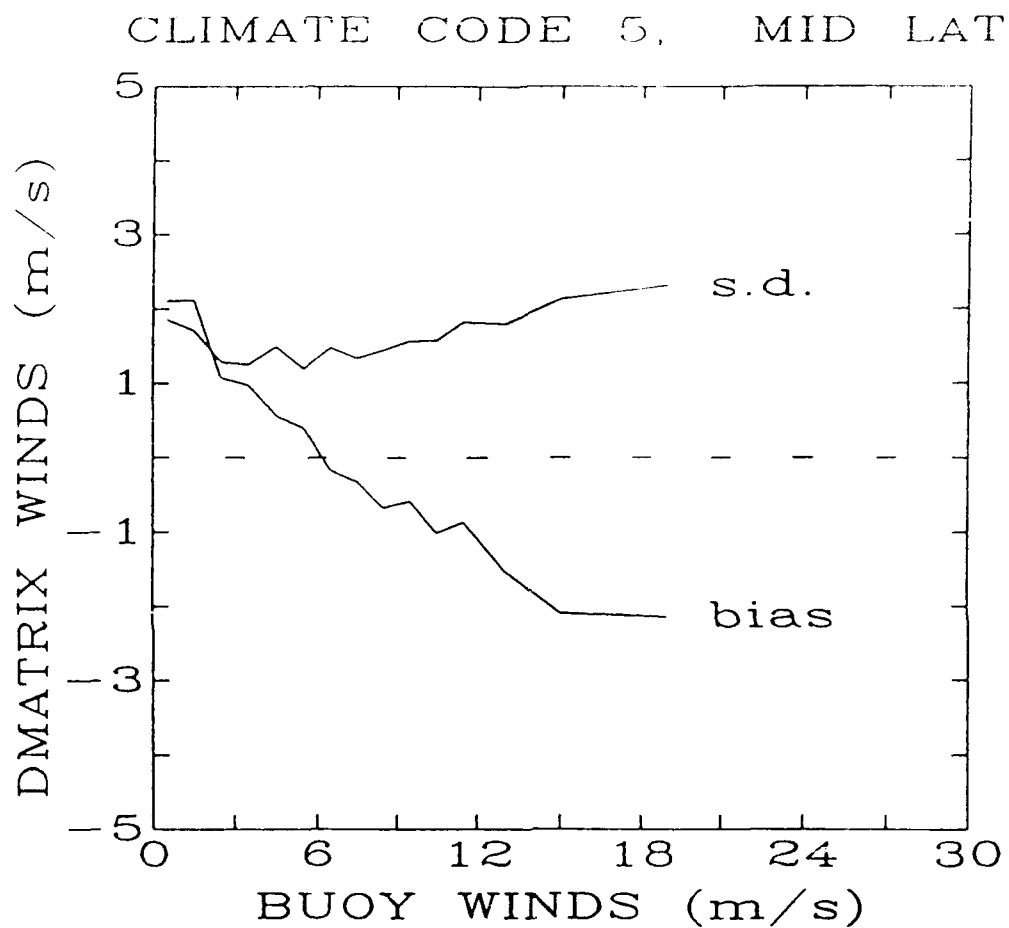


Fig. 3.1 Standard deviation (ie. random error), SD, and bias of the SSM/I wind speed retrievals from the ERT D-matrix algorithm plotted as a function of the "true" wind speed measured by NOAA ocean buoys.

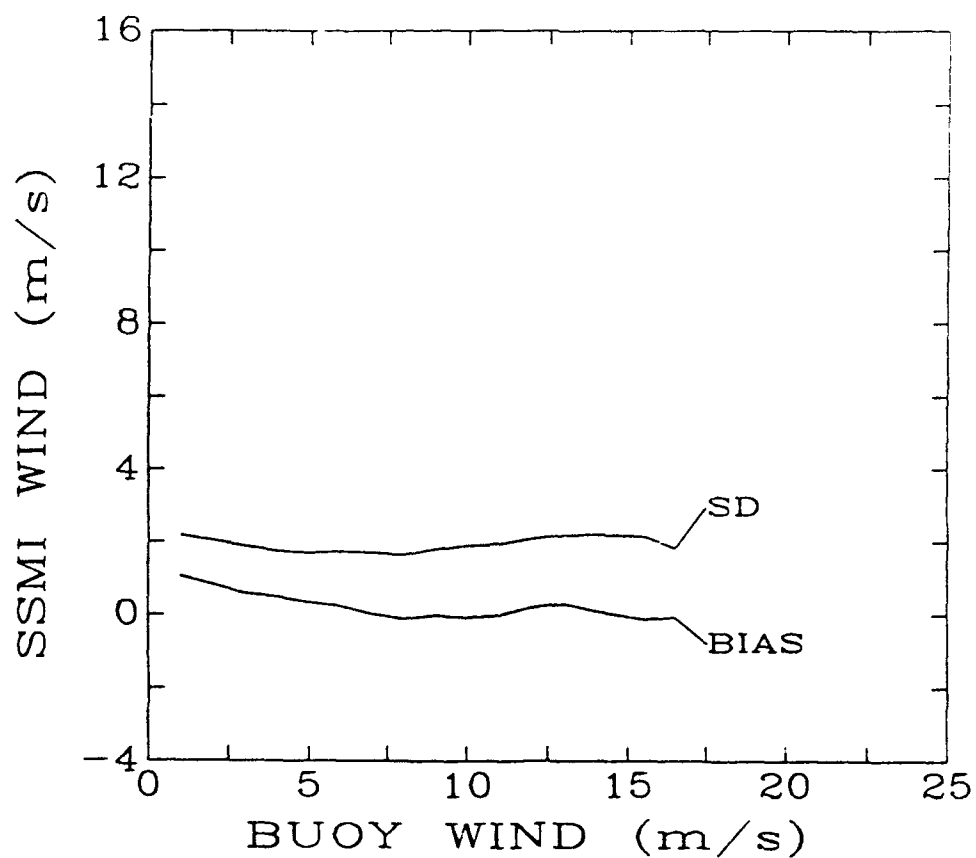


Fig. 3.2 Standard deviation (ie. random error), SD, and bias of the SSM/I wind speed retrievals from the Global D-matrix algorithm plotted as a function of the "true" wind speed measured by NOAA ocean buoys. The SSM/I brightness temperature difference, $T_D(37V) - T_B(37H)$, for data used to create this plot was always greater than 52 K.

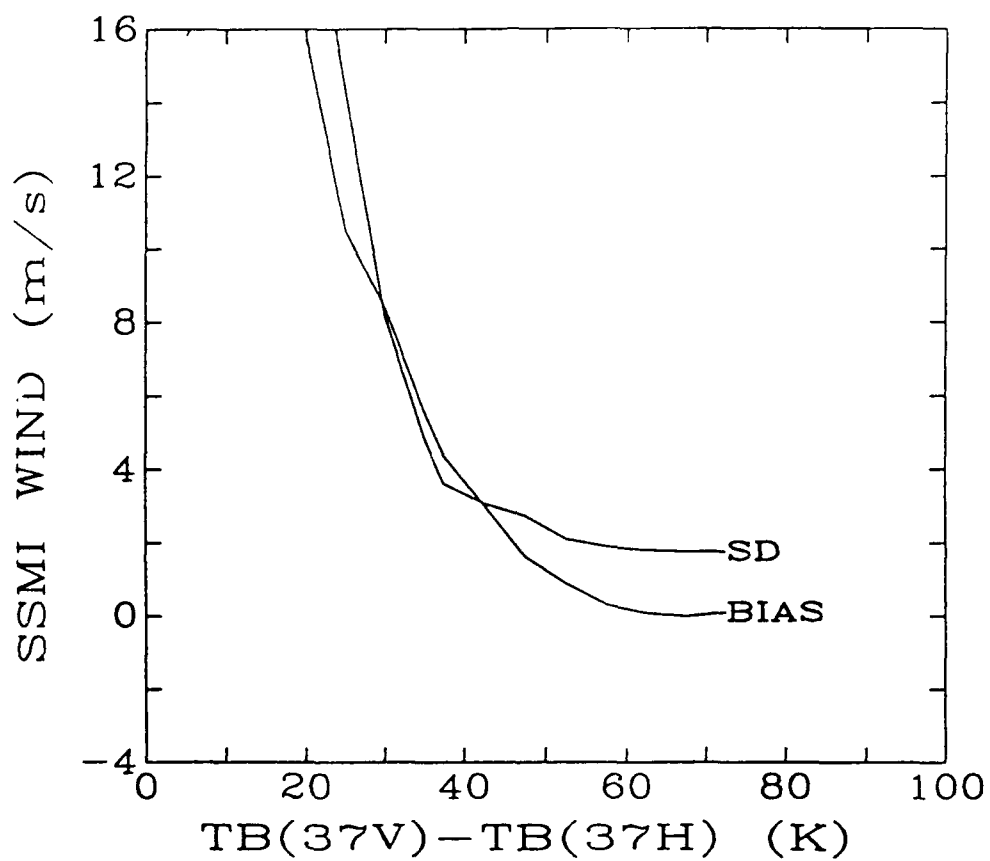


Fig. 3.3 Standard deviation (ie. random error), SD, and bias of the SSM/I wind speed retrievals from the Global D-matrix algorithm plotted as a function of the the SSM/I brightness temperature difference, $T_B(37V) - T_B(37H)$.

mathematically described as follows,

$$\text{weather-bias (m/s)} \approx \frac{18.56 - W_T}{(\Delta_{37} - 30.7)^4} \quad (3.1)$$

where W_T is the true surface wind in m/s .

Note that the statistical interpretation of the accuracy flags given in section 2 is strictly valid only under accuracy flag 0 conditions when the retrieval bias (ie. weather-bias) is zero. However, a more severe problem attributable to the weather-bias is that it leads to ambiguous retrievals; a fact that is demonstrated by the following example. Consider the situation where W_T is equal to 19 m/s and the associated value of the Δ_{37} differential is 30 K . Using $\Delta_{37} = 30$ and $W_T = 3$ in equation (3.1) gives a weather-bias of 17 m/s , therefore the Global D-matrix estimate, W_G , of the wind speed is $17 + 3 = 20$ m/s . Similarly, using $\Delta_{37} = 30$ and $W_T = 10$ in (3.1) gives a weather-bias of 9.4, indicating that W_G is 19.4 m/s . Finally, using $\Delta_{37} = 30$ and $W_T = 19$ in (3.1) gives a weather-bias of -0.5, indicating that W_G is 18.5 m/s . One can see from this example that when Δ_{37} is equal to 30 K , the Global D-matrix estimates the surface wind to be approximately 19 m/s regardless of the true wind. The fact that W_G is approximately equal to W_T when W_T is 19 m/s is just coincidence and not useful in an operational sense. We believe, along with others, [Holliday and Waters, 1989] [Rao et al., 1989], that the Global D-matrix algorithm does not fully exploit the wind speed measuring capability of the SSM/I. Furthermore, we consider the weather-bias to be the major deficiency of the Global D-matrix algorithm. Therefore, removal of the weather-bias is necessary in order to realize the full wind speed measuring potential of the SSM/I and considered to be the primary goal of this study.

There is interest in using SSM/I estimates of over-ocean wind speed to monitor hurricanes, typhoons and tropical storms [Holliday and Waters, 1989], [Rappaport, 1991]. Accurate SSM/I estimates of the winds in the core regions of these storms is not possible due to the heavily water laden atmosphere and the spatial resolution of the SSM/I. However, SSM/I estimates of the 20 m/s (40 knot) wind speed radius for these storms may be possible once the weather-bias problem has been solved. A second important step towards achieving this goal is to verify the high wind (> 12 m/s) accuracy of SSM/I wind speed estimates. Although the National Oceanic and Atmospheric Administration (NOAA) ocean-buoy data base used during the DMSP Cal/Val effort to create and test the Global D-matrix algorithm contained some high wind measurements, they were mostly under accuracy flag 1, 2 and 3 conditions. Since the DMSP Cal/Val effort concentrated on winds in accuracy flag 0 conditions, where very few high wind comparisons were available, the high wind retrieval accuracy was not specified. In addition we have augmented the buoy data with high wind speed measurements made by the Stepped Frequency Microwave Radiometer (SFMR) which is owned by the Microwave Remote Sensing Laboratory (MIRSL) at the University of Massachusetts and routinely flies aboard NOAA aircraft on hurricane reconnaissance missions. The SFMR wind speed measurements together with those of the NOAA buoy network provide the data needed to validate the ability of the SSM/I to measure the 20 m/s wind speed radius of hurricanes, tropical storms and typhoons.

In summary, the goals of this study are to create an improved wind speed retrieval

algorithm which does not suffer from a weather-bias and to validate the retrieval accuracy of the algorithm for winds up to at least 20 m/s.

4. Methodology

The purpose of this section is to define terminology and graphical techniques used throughout this report and to describe the statistical approach used to create new SSM/I wind speed retrieval algorithms.

Creation of a wind speed retrieval algorithm begins with the collection of a "merged data set" composed of coincident pairs of SSM/I measured brightness temperatures and surface measurements of the true wind made by well calibrated "ground-truth" instruments. The wind and brightness temperatures are paired according to a "comparison criteria" which helps insure that the SSM/I and the ground truth instrument are "seeing" the same wind field. The ground-truth instruments used for this study are NOAA buoys and the MIRSLS SFMR. The associated comparison criteria is described in section 5.

The merged data set is randomly divided into two subsets called the "training" and "testing" sets. The new algorithm is created using various statistical regression techniques [Draper and Smith, 1981] and data from the training set. The new algorithm is then validated using data of the testing set. Our testing procedure makes extensive use of "residual" plots such as the one shown in Figure 4.1. Residual plots derive their name from the fact that the vertical axis of the plot always indicates the algorithm residual which is defined as the difference between the algorithm retrieved winds and the ground-truth wind. The horizontal axis of the residual plots used in this study indicate either the ground-truth wind speed or the SSM/I brightness temperature difference, Δ_{37} .

In order to more clearly convey the information found in the residual plot we often show instead the "interpreted residual plot". The interpreted residual plot is obtained by dividing the region of the residual plot into a number of vertical bins and calculating the statistical average (labelled BIAS in the plot) and the standard deviation, SD, about the average of the points falling within each bin. In practice, calculation of the SD and BIAS for the interpreted residual plot is an iterative process involving removal of "outlier" points. More specifically, the first step is to calculate the SD and BIAS for a particular bin and then remove data points (outliers) whose associated bias is equal to more than 5 times the bin SD. The SD and BIAS are then recalculated for the data of the bin without using the outliers identified in the first step.

The interpreted residual plot corresponding to the residual plot of Figure 4.1 is shown in Figure 3.3 and was used to study the weather-bias of the Global D-matrix algorithm. Figure 3.2 shows the interpreted residual plot used to study the wind speed bias of the Global D-matrix algorithm. The interpreted residual plot shown in Figure 3.3 was also used to define the Global D-matrix accuracy flags. The first step in defining the flags was to select accuracy bands, which were decided upon during the DMSP Cal/Val effort to be 0-2 m/s, 2-5 m/s, 5-10 m/s and > 10 m/s. The next step is to use Figure 3.3 and locate the values of Δ_{37} at which the SD curve passes through 2, 5 and 10 m/s. The four regions defined by these three values of Δ_{37} correspond to the Δ_{37} extent of each accuracy flag.

The format of the retrieval algorithms used in this study can be classified as either the "multiple version linear" type or the "single-version nonlinear" type. The multiple-version

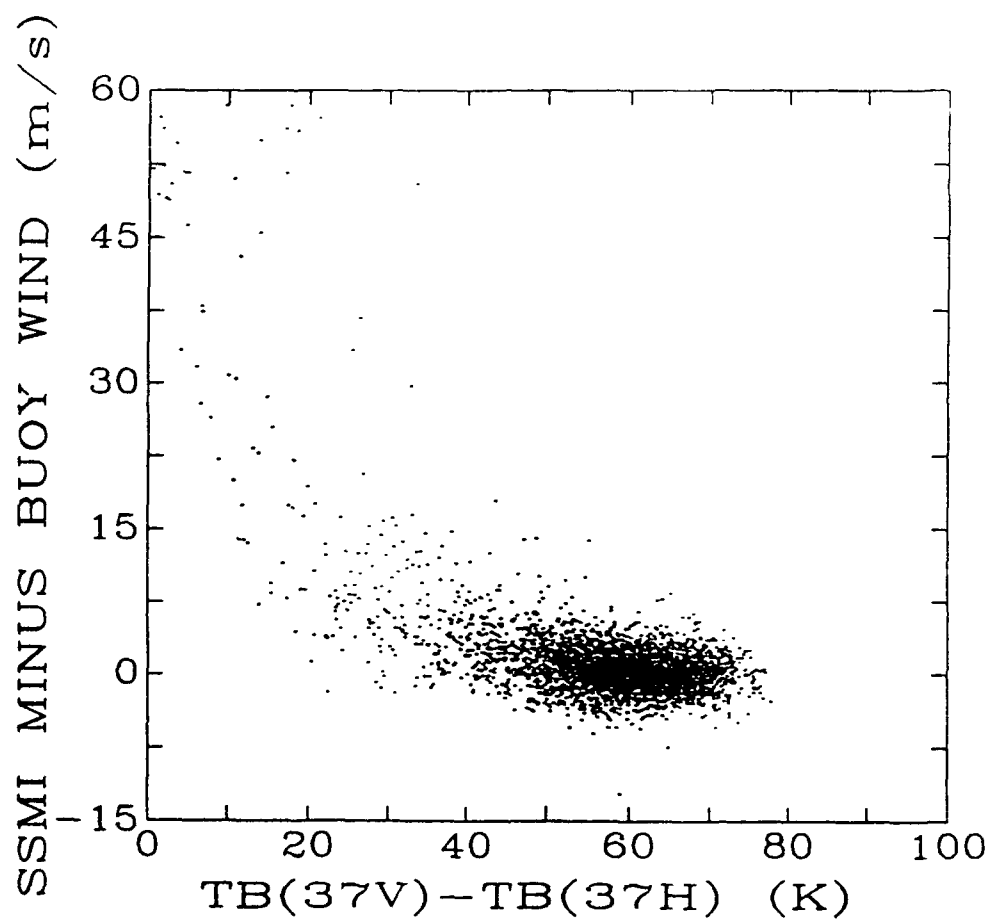


Fig. 4.1 The difference between SSM/I and NOAA buoy measured wind speed plotted against the SSM/I brightness temperature difference, $T_B(37V) - T_B(37H)$, for the 3982 data pairs of the SSM/I-buoy merged data file.

linear type is the format suggested by ERT and used in the original D-matrix algorithm. This type algorithm derives a wind speed estimate, W , from an equation which is a linear combination of selected SSM/I brightness temperature measurements, $T_B(i)$ as shown in equation (4.1) below,

$$W = D_0 + \sum_{i=1}^N D_i T_B(i) \quad (4.1)$$

where the D_i are constants to be determined. The "multiple version" portion of the title refers to the fact that this type of algorithm is in fact several algorithms; each valid only under a specific set of conditions (environmental, seasonal, geographical etc.).

The "single-version nonlinear" type algorithm derives a wind speed estimate from an equation which can have both linear and nonlinear terms containing selected $T_B(i)$. The "single version" portion of the title refers to the fact that this is a single algorithm valid under all conditions. An example this type of this type of algorithm will be discussed in section 7.

5. Merged Data Set and Comparison Criteria

The data base used to validate/repair the SSM/I wind speed algorithm is composed of "data pairs" each consisting of SSM/I brightness temperature measurements which are collocated with measurements of wind speed made by selected NOAA buoys or with measurements of wind speed made by the Stepped Frequency Microwave Radiometer (SFMR) [Jones et al, 1981]. The method of comparing SSM/I and NOAA buoy measurements of wind speed is described by [Goodberlet et al., 1989] and the histograms in Figures 5.1 and 5.2 indicate the distribution of SSM/I Δ_{37} and buoy wind speed associated with the 3982 data pairs of this merged data set. The method of comparing SSM/I and SFMR wind speed measurements is described below.

Since the SSM/I and SFMR footprints (size of the ocean area being observed) differ considerably, direct comparison of the wind speed measurements from each instrument is not possible. Instead, one must use a group of SFMR measurements which together "see" the same ocean area as the SSM/I. More specifically, the following comparison criteria was used in pairing SSM/I and SFMR wind speed measurements.

- a. A weighted average of the approximately 30 SFMR wind speed measurements which fall within an SSM/I footprint are compared directly to the SSM/I wind speed retrieval. Weights are inversely proportional to the SFMR footprint distance from the center of the SSM/I footprint.
- b. If less than 30 SFMR footprints fall within a SSM/I footprint then the SFMR passed only along the edge of the SSM/I footprint and no comparison is made.
- c. The SFMR measurement must be made within 2 hours of the SSM/I measurement.

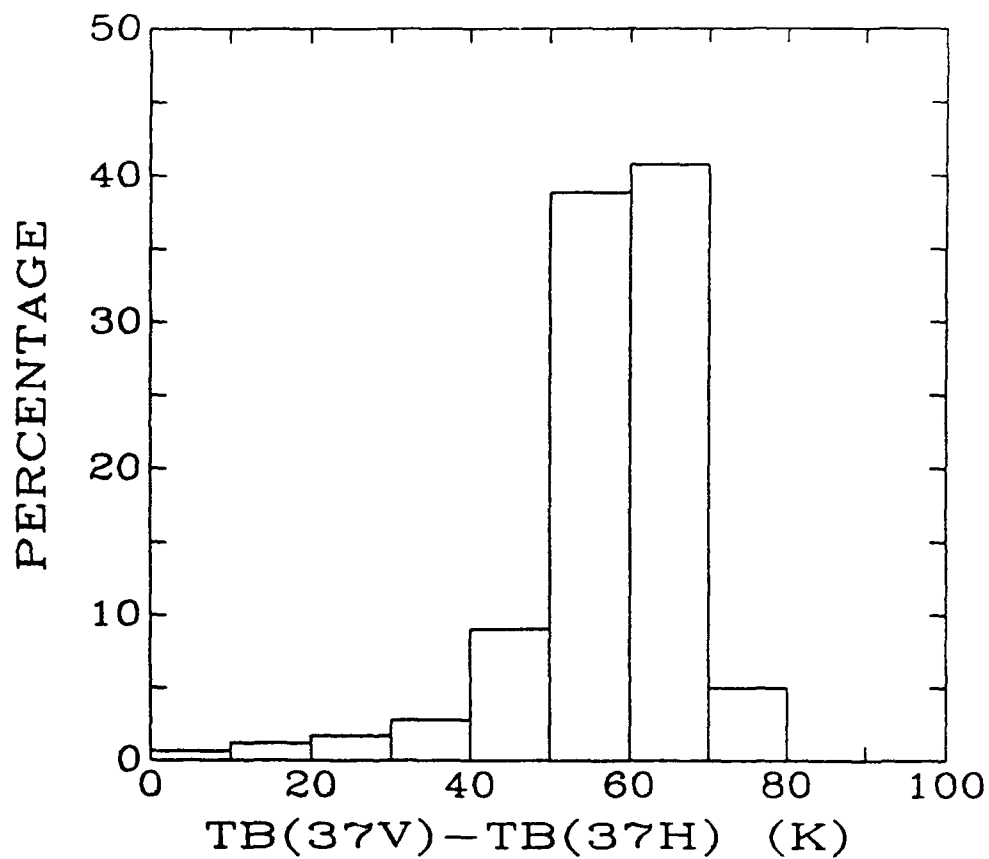


Fig. 5.1 Histogram of SSM/I brightness temperature difference, $T_B(37V) - T_B(37H)$, for the 3982 data pairs of the SSM/I-NOAA buoy merged data file.

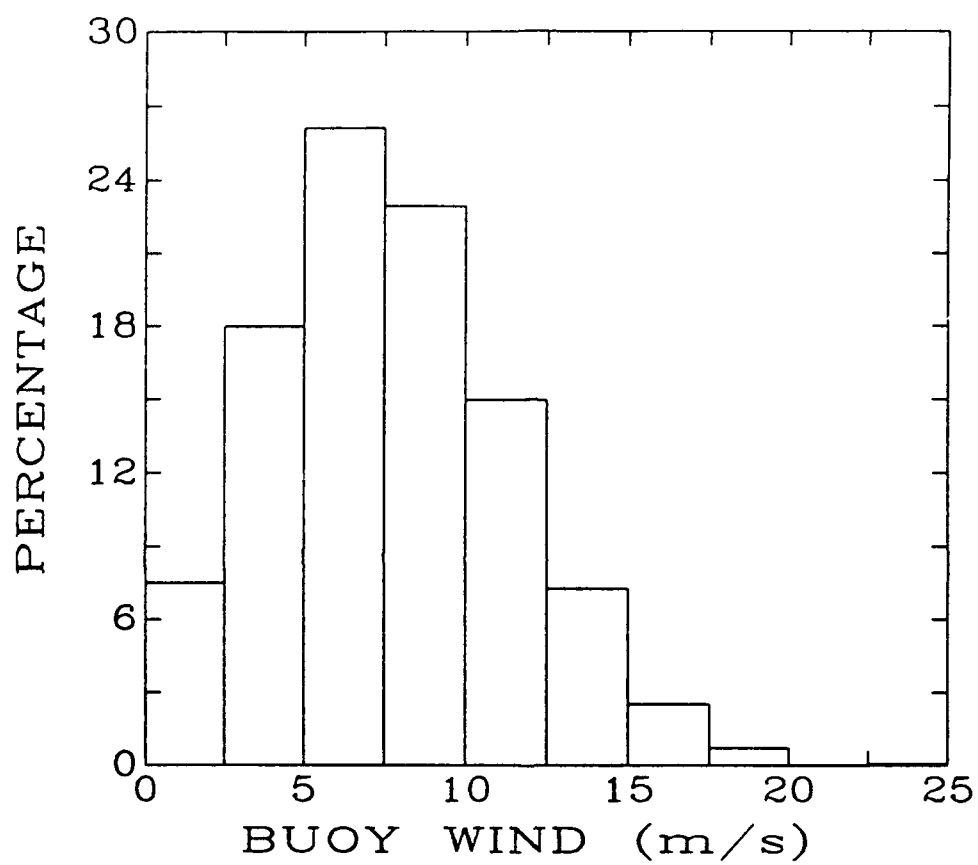


Fig. 5.2 Histogram of the NOAA buoy measured wind speed for the 3982 data pairs of the SSM/I-buoy merged data file.

- d. SFMR winds, referenced to a height of 10 meters, were converted to the D-matrix reference height of 19.5 meters assuming a standard logarithmic wind speed profile.
- e. To prevent land contamination of ocean brightness temperatures and to insure that the land did not restrict the wind speed fetch distance necessary for creating fully developed seas, only SFMR measurements further than 100 km from land were used. The effect of limited fetch on the SSM/I wind speed measurements was recently discussed by [Glazman, 1991].

Using the above comparison criteria, approximately 200 coincident measurements of SSM/I and SFMR wind speed were obtained from seven SFMR overflights of four tropical cyclones and one SFMR overflight of an upper latitude cyclone located near the gulf of Alaska. The eight SFMR overflights are described in Table 2. The histograms shown in Figures 5.3 and 5.4 indicate the distribution of SSM/I Δ_{37} and SFMR wind speed associated with the 200 data pairs of this merged data set.

6. SFMR Calibration

The reported wind speed retrieval accuracy of the SFMR is approximately 2 m/s for winds in the range of 15 m/s to 55 m/s and less than 2 m/s for winds below 15 m/s [Black and Swift, 1984]. Calibration of the SFMR was checked at least once during each of the flights shown in Table 2 by comparing SFMR winds with one of the following alternate wind speed measurements:

- a. Wind speed measurements made by ocean buoys that fell near the NOAA aircraft flight path.
- b. Aircraft measured winds which were converted from the aircraft altitude to a height of 10 meters above the ocean surface.
- c. SSM/I D-matrix medium range (10–18 m/s) wind speed retrievals from areas where the Δ_{37} differential was greater than 45 K.

7. Results

Although we have investigated new SSM/I wind speed retrieval algorithms of both the "multiple-version linear" and "single-version nonlinear" types, we have found the "single-version nonlinear" approach to be superior. The main reason for choosing the latter is that it does not suffer from the discontinuities associated with switching between multiple algorithms. Additionally the "single-version nonlinear" approach better accounts for the fact that a water laden atmosphere makes the wind speed retrieval process inherently nonlinear. The behavior of the weather-bias, which is graphically shown in Figures 7.1 through 7.3, was used to determine the format of the new algorithm. Unlike Figure 3.3 which shows the weather-bias for *all* wind speed ranges, Figures 7.1 through 7.3 show the weather-bias for the low (0–6 m/s), medium (6–12 m/s) and high (above 12 m/s) wind speed ranges separately. Additionally, Figure 7.4 shows the weather-bias behavior associated with comparisons of SSM/I and SFMR under high (above 15 m/s) wind

Table 2. Stepped Frequency Microwave Radiometer (SFMR) flights which were collocated with wind speed measurements of the Special Sensor Microwave/Imager (SSM/I).

<u>Storm</u>	<u>Date</u>	<u>Time (Zulu)</u>	<u>Latitude Range (N)</u>	<u>Longitude Range (W)</u>
Emily	24Sep87	1815-0320	20-39	64-80
Alaska	01Dec87	1100-1930	40-54	121-138
Florence	08Sep88	1830-0315	17-26	77-93
Florence	09Sep88	1600-0100	24-30	79-91
Gilbert	13Sep88	1615-0045	16-26	78-86
Gilbert	15Sep88	0930-1840	19-26	80-93
Gilbert	15Sep88	2200-0700	17-29	79-96
Hugo	15Sep89	1615-2015	11-16	52-59

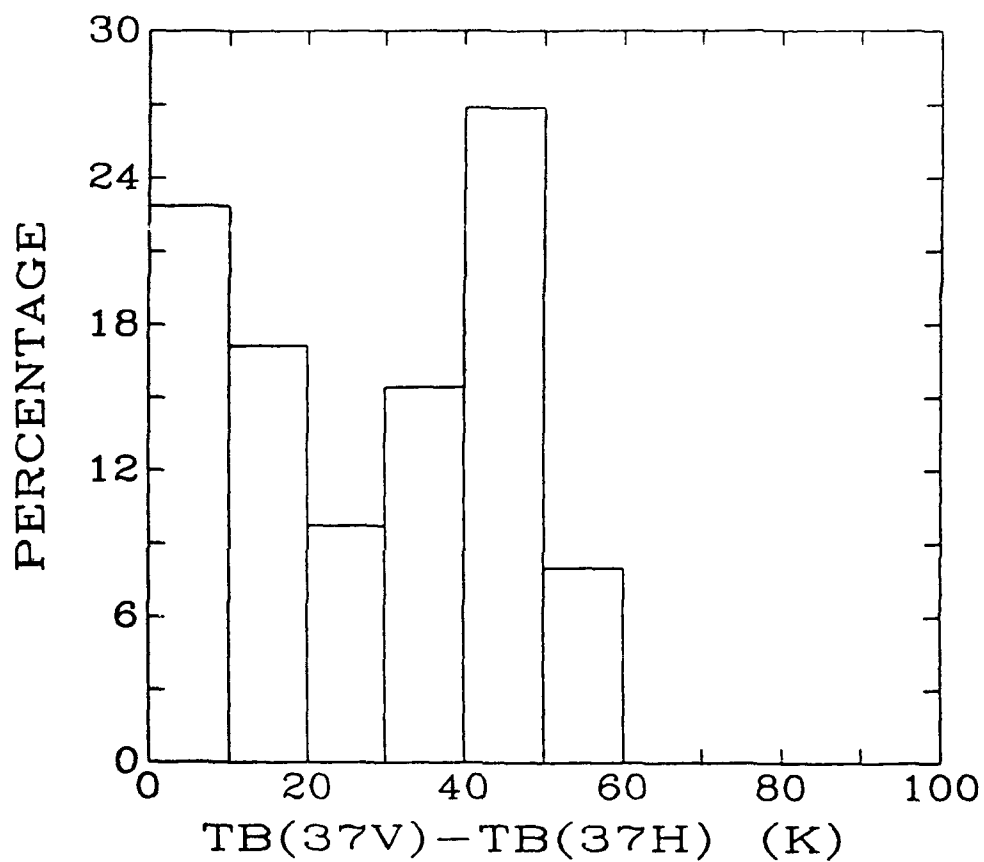


Fig. 5.3 Histogram of SSM/I brightness temperature difference, $T_B(37V) - T_B(37H)$, for the 200 data pairs of the SSM/I-SFMR merged data file.

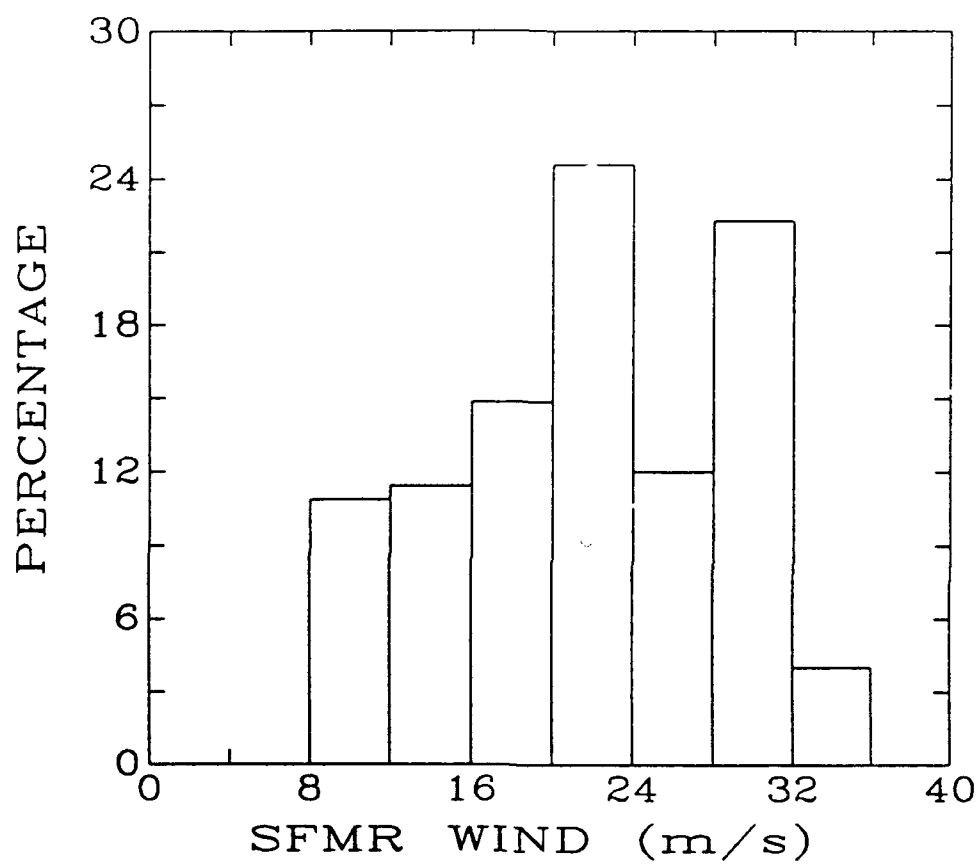


Fig. 5.4 Histogram of the SFMR measured wind speed for the 200 data pairs of the SSM/I-SFMR merged data file.

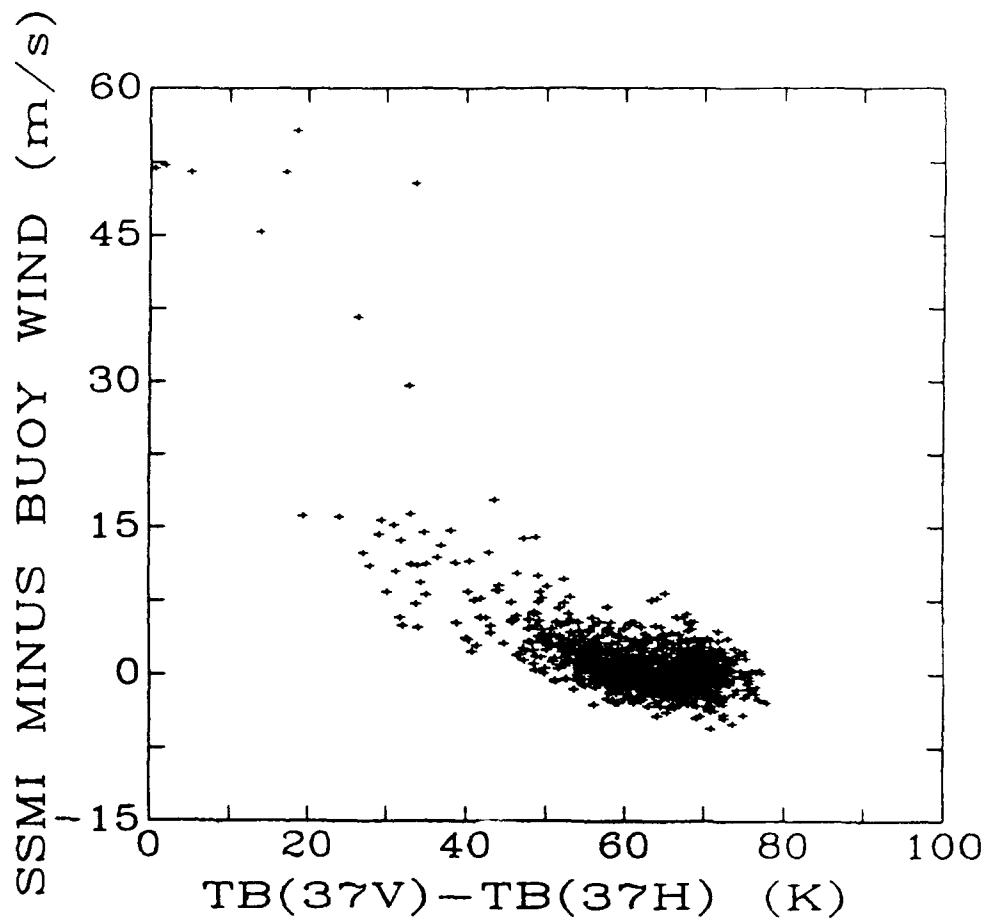


Fig. 7.1 The difference between SSM/I and NOAA buoy measured wind speed plotted against the SSM/I brightness temperature difference, $T_B(37V) - T_B(37H)$, for the 1442 data pairs of the SSM/I-buoy merged data file where the buoy measured wind speed is between 0 and 6 m/s.

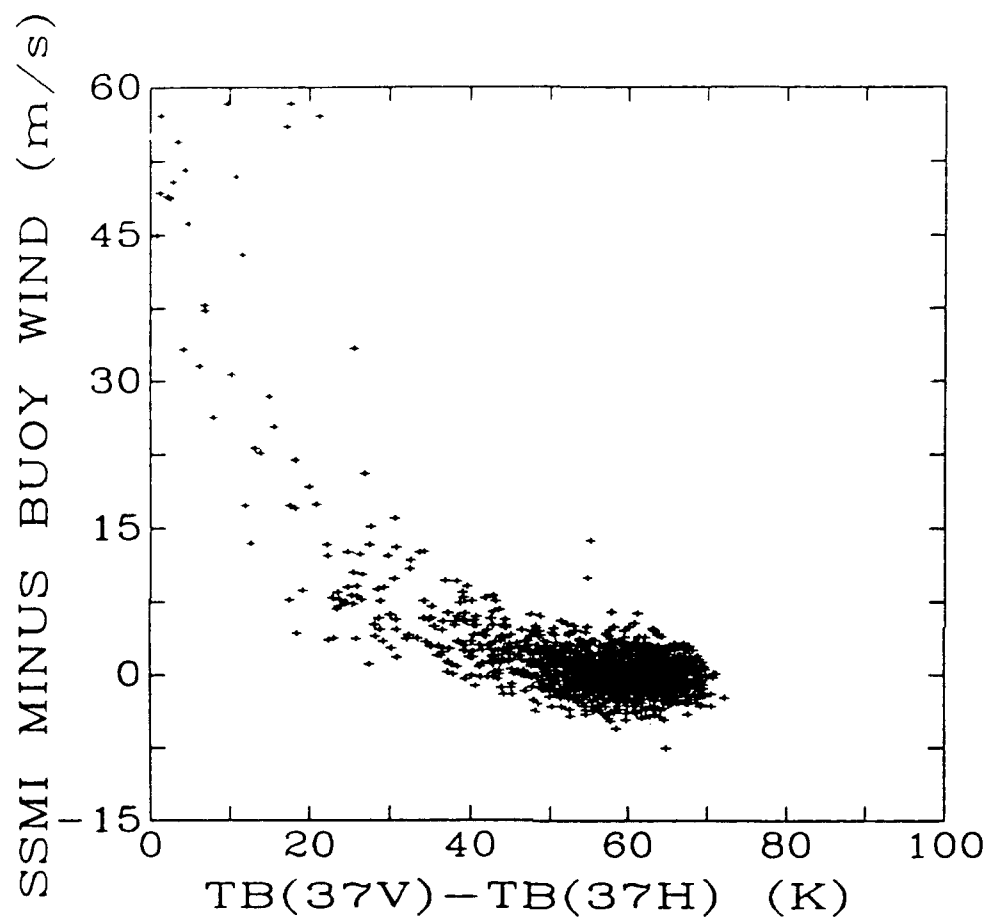


Fig. 7.2 The difference between SSM/I and NOAA buoy measured wind speed plotted against the SSM/I brightness temperature difference, $T_B(37V) - T_B(37H)$, for the 2044 data pairs of the SSM/I-buoy merged data file where the buoy measured wind speed is between 6 and 12 m/s .

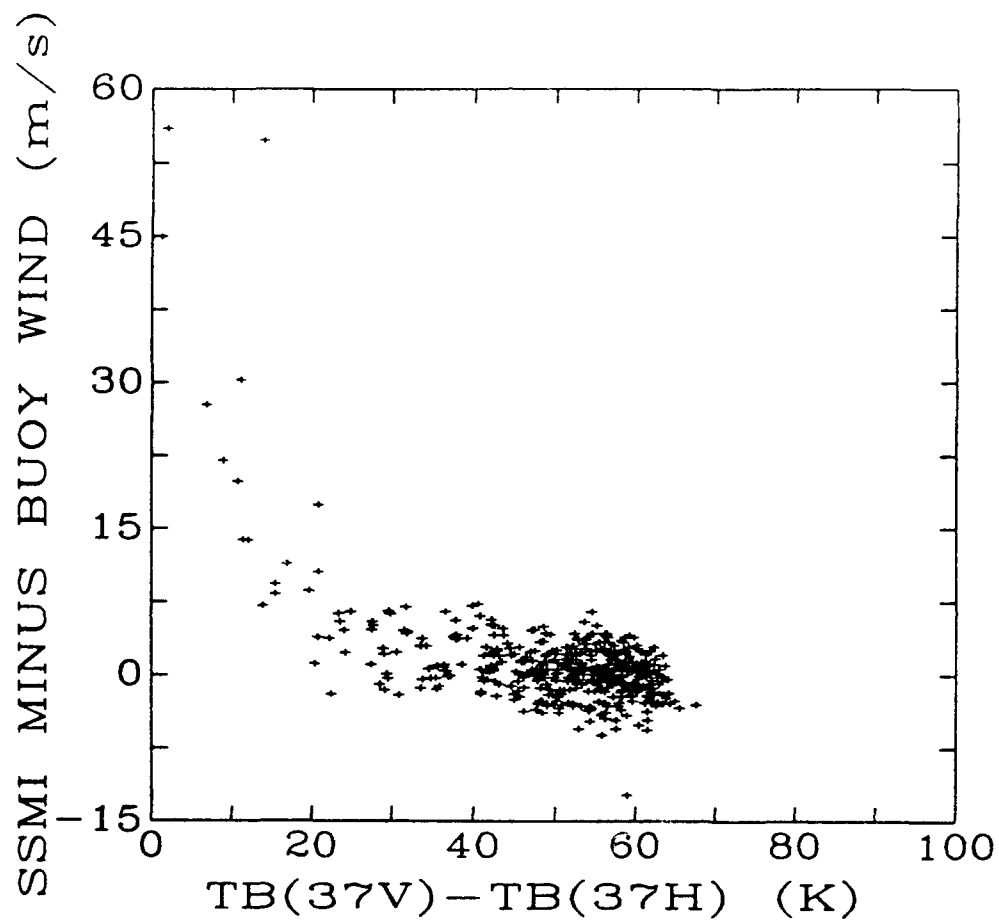


Fig. 7.3 The difference between SSM/I and NOAA buoy measured wind speed plotted against the SSM/I brightness temperature difference, $T_B(37V) - T_B(37H)$, for the 496 data pairs of the SSM/I-buoy merged data file where the buoy measured wind speed is greater than 12 m/s .

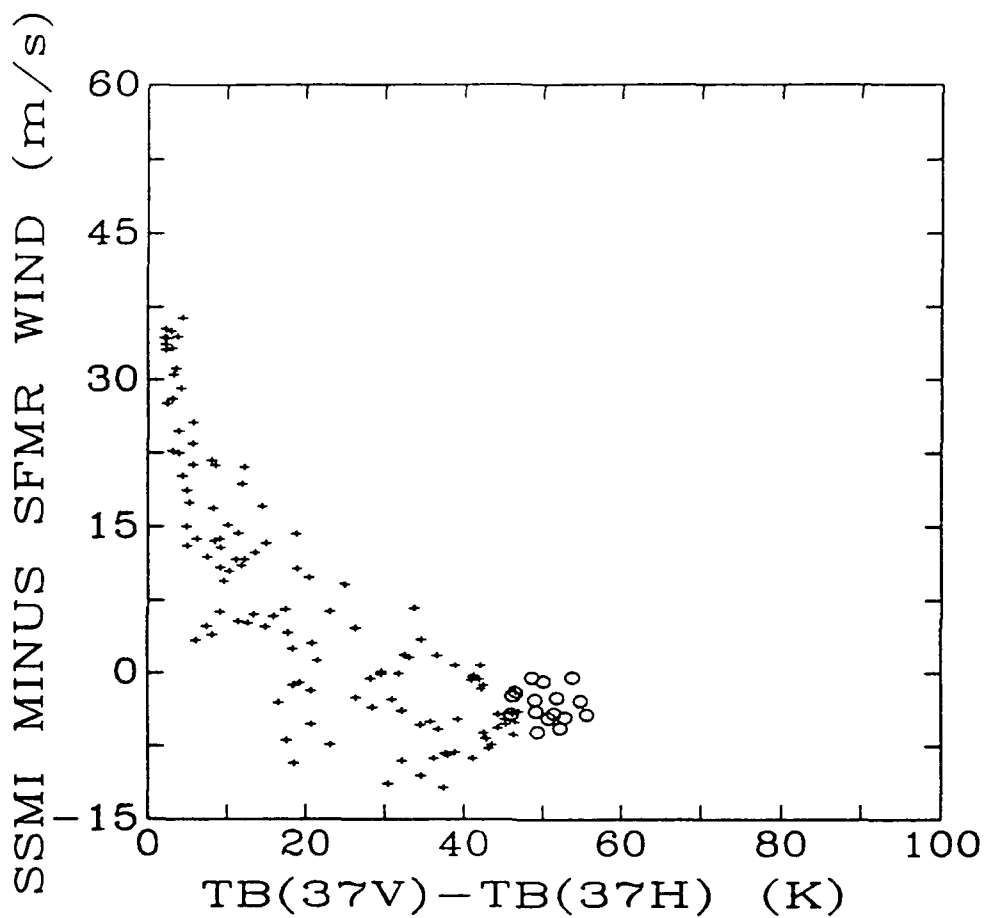


Fig. 7.4 The difference between SSM/I and SFMR measured wind speed plotted against the SSM/I brightness temperature difference, $T_B(37V) - T_B(37H)$, for the 140 data pairs of the SSM/I-SFMR merged data file where the SFMR measured wind speed is greater than 15 m/s. The "+" marks indicate data from tropical regions and the "o" marks indicates data from a storm near the Gulf of Alaska (see Table 2)

conditions. It is interesting to note from these figures that the weather-bias is greater for low winds than for high winds. Mathematically one can describe the weather-bias, $W_G - W_T$, as follows,

$$W_G - W_T \simeq \frac{B_1 - W_T}{(\Delta_{37}/B_2)^N} \quad (7.1)$$

where W_G is a wind speed retrieval from the Global D-matrix algorithm. W_T is the ground-truth wind (as measured by the NOAA buoys or the SFMR), and B_1 , B_2 , N are constants to be determined.

Our attempts to remove the weather-bias from Global D-matrix retrievals in all wind speed ranges have not been successful however, removal of the weather-bias from retrievals made under high and medium wind speed conditions and a significant reduction of the weather bias for retrievals made under low wind speed conditions was found to be possible. The procedure for creating this new algorithm was to first use a weighted Minimum Squared Error (MSE) technique [Draper and Smith, 1981] and a "training" data set composed of the SSM/I-buoy data pairs with an associated Δ_{37} differential of between 20 and 54 K to solve for the coefficients, B_1 , B_2 , and N shown in equation (7.1). The weights used in the regression are obtained from the wind speed density function associated with the training set and have the effect of making all wind speed ranges equally important in the creation of the new algorithm. Secondly, solving equation (7.1) for W_T results in the specific format of the new algorithm which is called the GSW algorithm. Details of the GSW algorithm are given in Table 3.

Figures 7.5 through 7.7 give the performance of the GSW algorithm under the conditions of high, medium and low winds and were used, as described in section 4, to establish the accuracy flag criteria. Note that the GSW algorithm accuracy flag criteria is based solely on the value of Δ_{37} and no longer depends on the value of $T_B(19H)$. We have made this change since Δ_{37} alone seems capable of indicating the accuracy level of the algorithm retrievals. Additionally, we have defined, in Table 3, an "accuracy equation" as an alternative method of expressing the relationship between the GSW algorithm retrieval accuracy and the value of Δ_{37} .

The plots in Figures 7.8 and 7.9 were made to check whether the GSW algorithm is equally accurate at all latitudes. Figure 7.8 contains data from our most northern NOAA buoys (46035 at 57N,182E and 46001 at 56N,212E) collected during the period 1Sep87 through 1Mar88. See also [Schluessel and Luthardt, 1991] for upper latitude performance of the Global D-matrix algorithm. Since performance of the Global D-matrix algorithm and the GSW algorithm is essentially the same for a Δ_{37} differential of greater than 50 K, one can expect the two algorithms to perform equally well in the upper latitude regions where the Δ_{37} differential is usually greater than 50 K. Figure 7.9 contains data from two lower latitude buoys (42001 at 26N,270E and 42002 at 26N,266E) also collected during the period 1Sep87 through 1Mar88. Since these two plots show good agreement between the GSW algorithm retrievals and the buoy measurements, we conclude that the GSW algorithm accuracy is not significantly dependent upon geographical location.

Finally, the cross-plot of Figure 7.10 is presented as a alternate means of showing the high wind retrieval performance of the GSW algorithm. Figure 7.10 also shows the range of high wind comparisons contained in our merged data set.

Table 3. Specifications of the GSW wind speed algorithm where the calculated wind speed, W , is in meters per second and referenced to a height of 19.5 meters above the ocean surface. *Under no conditions should this algorithm be used when the Δ_{37} differential is less than 31 K*

$$W = \frac{W_G - 18.56 \cdot \alpha}{1.0 - \alpha}$$

where :

$$W_G = 147.90 + 1.0969 \cdot T_B(19V) - 0.4555 \cdot T_B(22V) + \\ - 1.7600 \cdot T_B(37V) + 0.7860 \cdot T_B(37H)$$

$$\alpha = \left(\frac{30.7}{\Delta_{37}} \right)^4$$

$$\Delta_{37} = T_B(37V) - T_B(37H)$$

<u>Accuracy Flag</u>	<u>Criteria</u>	<u>Accuracy(m/s)</u>
0	$\Delta_{37} > 55$	< 2
1	$35 < \Delta_{37} < 55$	$2 - 5$
2	$32 < \Delta_{37} < 35$	$5 - 10$
3	$\Delta_{37} < 32$	> 10

or

$$\text{Accuracy (m/s)} = \frac{1.8}{1.0 - \alpha}$$

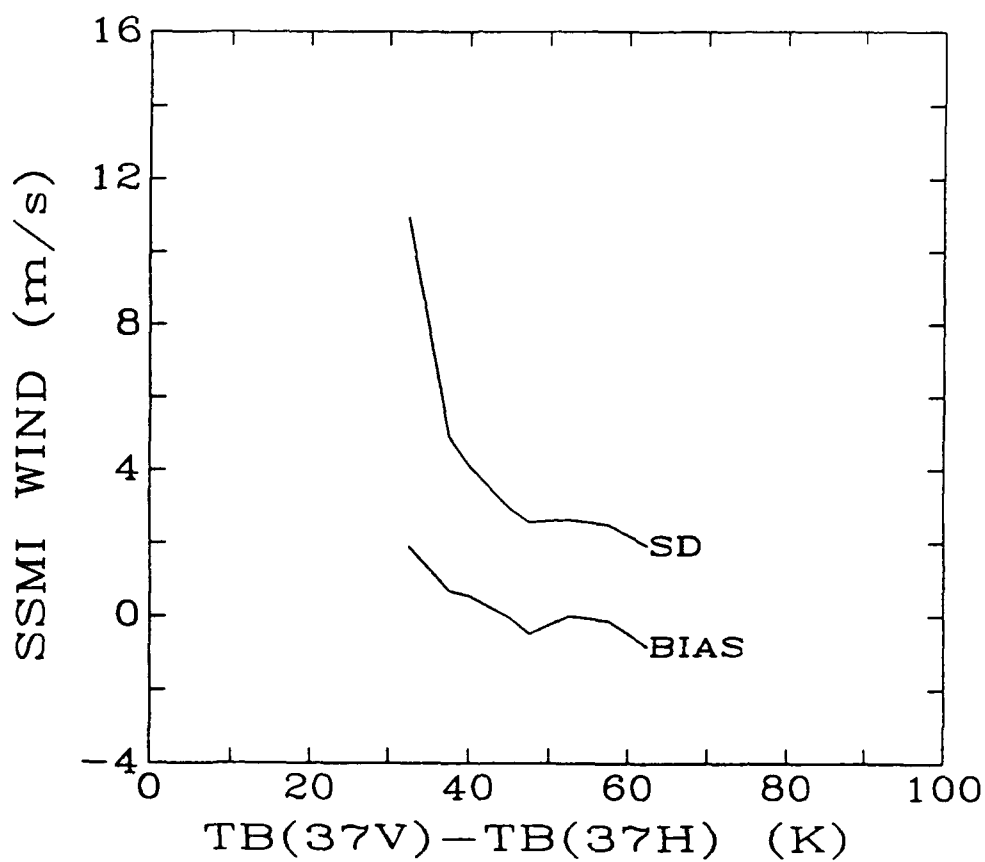


Fig. 7.5 Standard deviation (ie. random error), SD, and bias of SSM/I wind speed retrievals from the GSW algorithm made under high ($> 12 \text{ m/s}$) wind speed conditions plotted as a function of the SSM/I brightness temperature difference, $T_B(37V) - T_B(37H)$. Data used to construct this plot consisted of only SSM/I-buoy coincident data pairs.

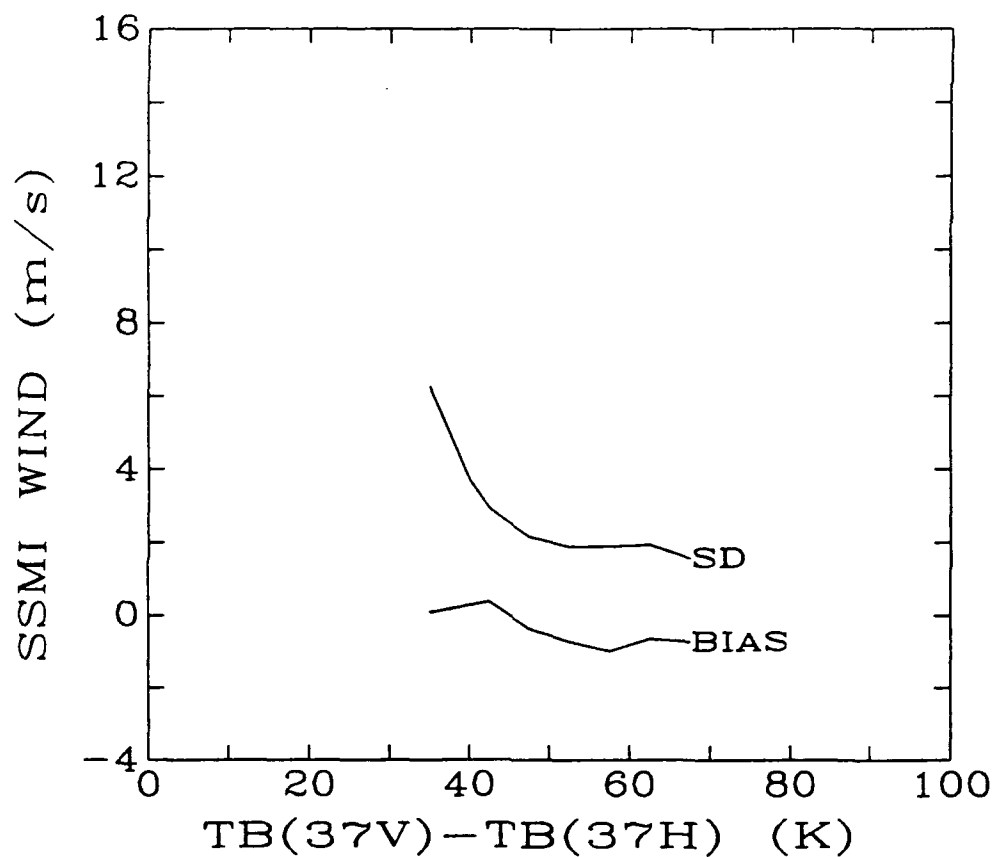


Fig. 7.6 Standard deviation (ie. random error), SD, and bias of SSM/I wind speed retrievals from the GSW algorithm made under medium (6–12 *m/s*) wind speed conditions plotted as a function of the SSM/I brightness temperature difference, $T_B(37V) - T_B(37H)$. Data used to construct this plot consisted of only SSM/I-buoy coincident data pairs.

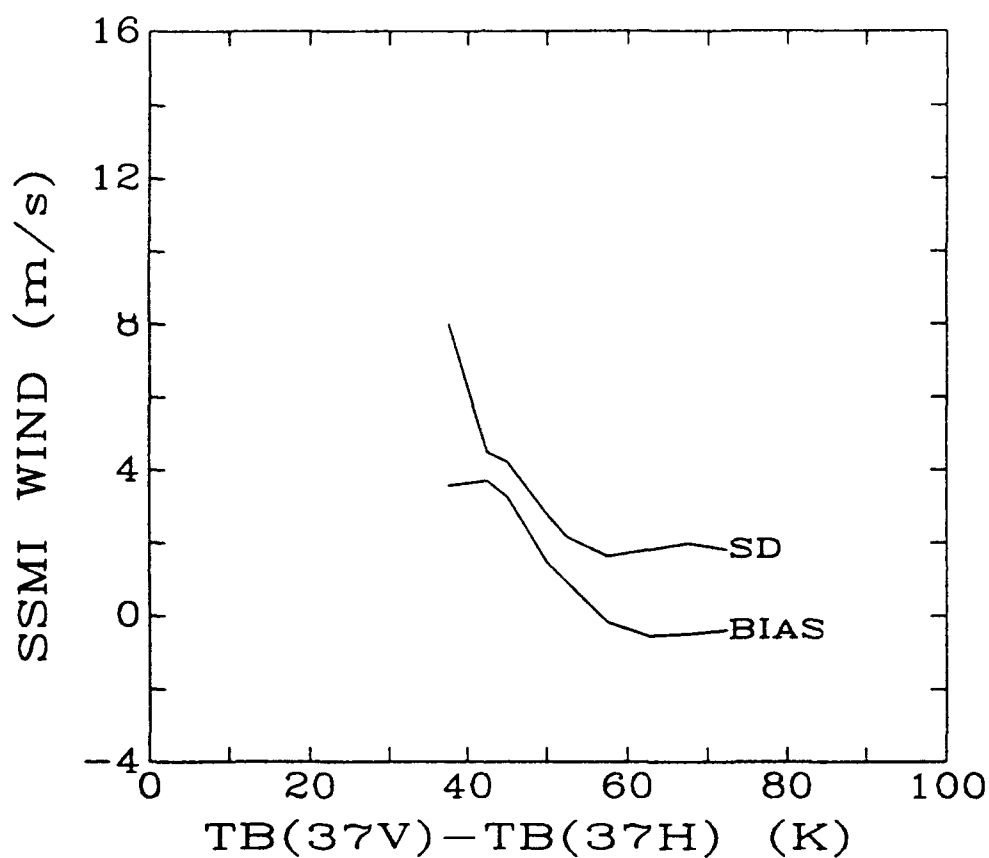


Fig. 7.7 Standard deviation (ie. random error), SD, and bias of SSM/I wind speed retrievals from the GSW algorithm made under low (0-6 m/s) wind speed conditions plotted as a function of the SSM/I brightness temperature difference, $T_B(37V) - T_B(37H)$. Data used to construct this plot consisted of only SSM/I buoy coincident data pairs.

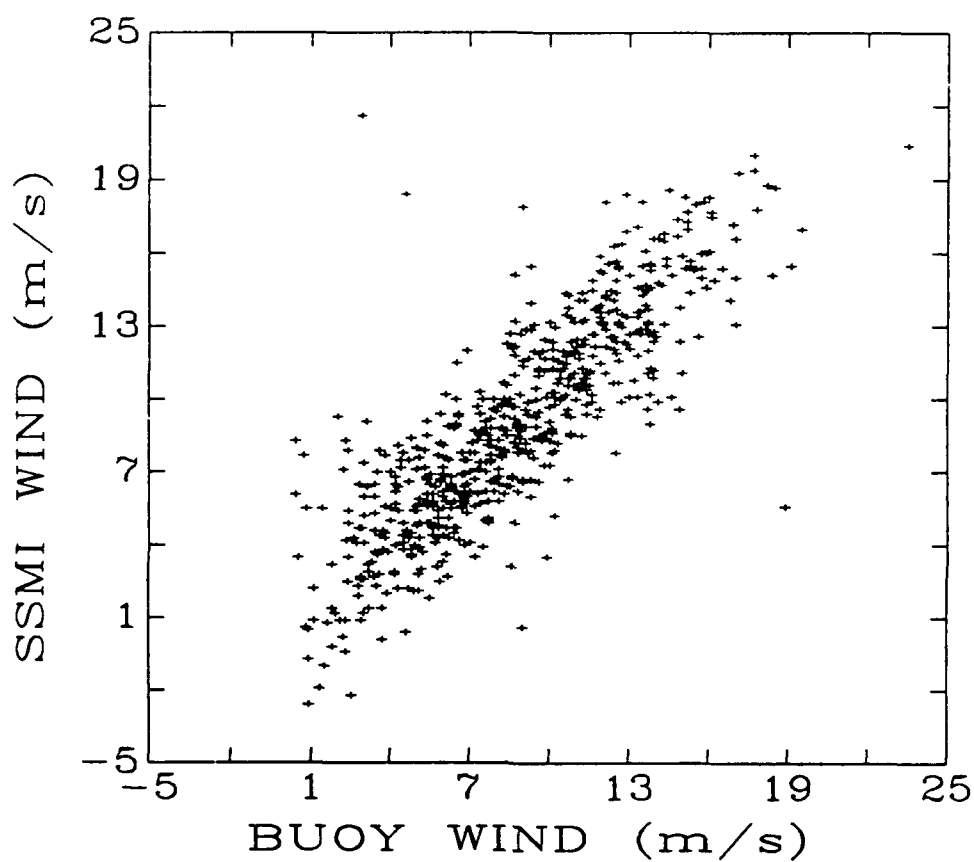


Fig. 7.8 Scatter-plot of SSM/I wind speed estimates from the GSW algorithm and coincident wind speed measurements from NOAA buoys 46035 and 46001 made during the time period 1Sep87 through 1Mar88. The SSM/I brightness temperature difference, $T_B(37V) - T_B(37H)$, for data used to create this plot was always greater than 35 K.

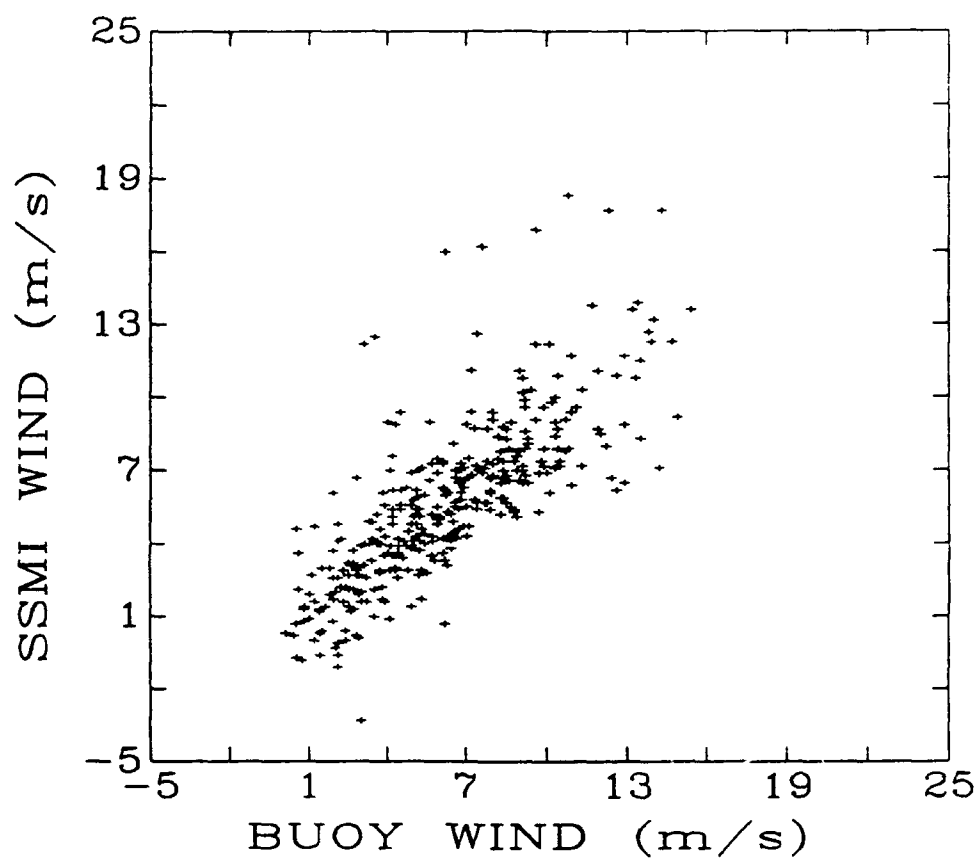


Fig. 7.9 Scatter-plot of SSM/I wind speed estimates from the GSW algorithm and coincident wind speed measurements from NOAA buoys 42001 and 42002 made during the time period 1Sep87 through 1Mar88. The SSM/I brightness temperature difference, $T_B(37V) - T_B(37H)$, for data used to create this plot was always greater than 35 K.

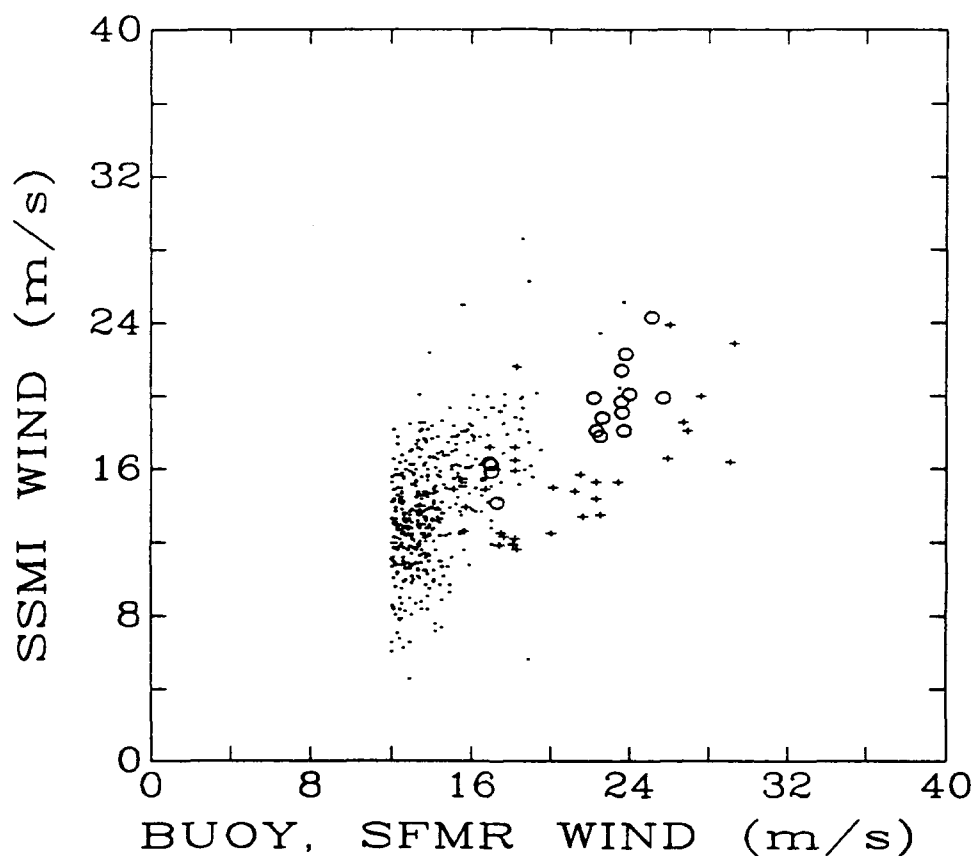


Fig. 7.10 Scatter-plot of SSM/I wind speed estimates from the GSW algorithm and coincident wind speed measurements made by NOAA buoys and the SFMR under high ($> 12 \text{ m/s}$) wind speed conditions. Points marked with a dot represent SSM/I-buoy comparisons. Points marked with a plus sign represent SSM/I-SFMR comparisons in tropical regions and points marked with a circle represent SSM/I-SFMR comparisons in a storm near the Gulf of Alaska (see Table 2). The SSM/I brightness temperature difference, $T_B(37V) - T_B(37H)$, for data used to create this plot was always greater than 35 K.

8. Discussion and Conclusions

In conclusion we feel that the GSW algorithm offers improved accuracy and a better understanding of the relationship between wind speed, Δ_{37} , and retrieval accuracy than the Global D-matrix algorithm. The GSW algorithm can be reliably used under conditions when the Δ_{37} differential is greater than 40 K and, with care, when Δ_{37} is greater than 35 K. Under these conditions the GSW algorithm gives unbiased estimates of medium to high winds (6-20 m/s) and tends to overestimate low winds (0-6 m/s) slightly. We do not recommend using the GSW algorithm when the Δ_{37} differential is less than 35 K and under no condition should it be used when the Δ_{37} differential is less than 31 K. It is our experience that the 20 m/s wind speed radius of some tropical storms and hurricanes lies in the region surrounding the storm where the Δ_{37} differential is greater than 35 K.

We are unable at this time to say whether the GSW wind speed retrievals are the best that can be obtained from the SSM/I data. The answer would result from a study of the physical process by which the SSM/I is able to sense changes in ocean surface wind speed and how this process is effected by a water-laden atmosphere. We recommend that investigations along such lines be initiated.

Finally, we note that the GSW algorithm can be reliably applied only to the F-8 SSM/I brightness temperature data. SSM/I's on other platforms will have slightly different calibration, making it necessary to modify the GSW algorithm or to adjust the brightness temperature calibration of the new SSM/I's to match that of the F-8 SSM/I.

Acknowledgements

Thanks to John Wilkerson and Eric Meindel of NOAA for providing us with the NOAA buoy data and to the National Snow and Ice Data Center for providing us with copies of the Frank Wentz Compact-TA tapes of SSM/I data. Additional thanks to Peter Black of NOAA and Karen St. Germain of the University of Massachusetts MIRSL for the SFMR data and assistance with the SFMR calibration and wind speed retrieval algorithm.

REFERENCES

- [1] Black, P.G. and C.T. Swift, Airborne Stepped Frequency Microwave Radiometer Measurements of Rainfall Rate and Surface Wind Speed in Hurricanes, Proc. 22nd Conf. Radar Meteorology, Amer. Meteorol. Soc., Boston, Ma., 433-438, 1984
- [2] Draper, N.R. and H. Smith, *Applied Regression Analysis*, 2nd ed., p. 108, John Wiley, New York, 1981
- [3] Glazman, R.E., Statistical Problems of Wind-Generated Gravity Waves Arising in Microwave Remote Sensing of Surface Winds, IEEE Trans. Geosci. Remote Sensing, 29, 135-142, 1991
- [4] Goodberlet, M.A., C.T. Swift and J.C. Wilkerson, Remote Sensing of Ocean Surface Winds With the Special Sensor Microwave/Imager, J. Geophys. Res., 94, 14,547-14,555, 1989
- [5] Holliday, C.R., and K.R. Waters, SSM/I Observation of Tropical Cyclone Gale Force Vicinity Winds, Proc. 4th Conf. Satellite Meteorology and Oceanography, Amer. Meteorol. Soc., San Diego, CA, 1989
- [6] Hollinger, J.P., DMSP Special Sensor Micro-wave/Imager Calibration/Validation, Naval Research Labs, Washington D.C., July 20, 1989
- [7] Jones, W.L., and P.G. Black, V.E. Delnore, C.T. Swift, Airborne Microwave Remote-Sensing Measurements of Hurricane Allen, Science magazine, 214, 274-280, 16 October 1981
- [8] Lo, R.C., A Comprehensive Description of the Mission Sensor Microwave Imager (SSM/I) Environmental Parameter Extraction Algorithm, Naval Research Labs memo. report 5199, Washington D.C., 1983
- [9] Rao, G.V., E.J. Ciardi and D.K. Rhudy, Comparison of SSM/I Rainrates and Surface Winds with the Corresponding Conventional Data in Northwest Pacific Typhoons, Proc. 4th Conf. Satellite Meteorology and Oceanography, Amer. Meteorol. Soc., San Diego, CA, 1989
- [10] Rappaport, E.N., Operational Applications of SSM/I Data at the National Hurricane Center, Proc. 19th Conf. Hurricane and Tropical Meteorology, Amer. Meteorol. Soc., Miami FL, 1991
- [11] Schluessel P., and H. Luthardt, Surface Winds Speeds Over the North Sea From Special Sensor Microwave/Imager Observations, J. Geophys. Res., 96, 4845-4853, 1991